PCCP

Accepted Manuscript

ROYAL SOCIETY OF CHEMISTRY

www.rsc.org/pccp

Physical Chemistry Chemical Physics
CREATED USING THE RSC LaTeX PCCP ARTICLE TEMPLATE – SEE www.rsc.org/electronicfiles FOR DETAILS
ARTICLE TYPE www. rsc.org/xxxxxx | XXXXXXXX

Switching Magnetic Interactions in the NiFe Prussian Blue Analogue : an *ab initio* Inspection

Tim Krah,[*a] **Nadia Ben Amor,**[b‡] **and Vincent Robert**[*a]

Received Xth XXXXXXXXXX 20XX, Accepted Xth XXXXXXXXX 20XX
First published on the web Xth XXXXXXXXXX 200X
DOI: 10.1039/b000000x

The magnetic interaction in the Ni(II)-Fe(III) Prussian Blue Analogue is investigated by means of Difference Dedicated Configuration Interaction (DDCI) calculations. Embedded cluster calculations are performed to extract the exchange coupling constant *J* with respect to an opening of the Ni-NC-Fe bridge while maintaining a rigid $Fe(CN)_6$ unit. It is shown that such active distortion significantly modifies the magnetic interaction scheme in the material. Not only a ferromagnetic to antiferromagnetic transition is observed, but the *J* value is varied from +11.4 cm^{-1} to -12.5 cm^{-1} when the Ni-Fe cyanide bridge is opened by 20° . The enhancement of the intersite hopping electron transfer integral by a factor of 1.5 can be correlated to the observed Na^+-ions mobility in a unified "cation-coupled electron transfer" (CCET) process. These results stress the complexity and originality of this class of compounds evidenced by the versatility of their magnetic network.

1 Introduction

Prussian Blue has received considerable attention as an inexpensive synthetic pigment ever since its synthesis at the beginning of the 18^{th} century.[1] On the other hand, Prussian Blue Analogues (PBA) owe their ongoing popularity to interesting physical and chemical properties such as spin-crossover, electron transfer or valence tautomerism.[2–4] PBAs contain one or two different transition metal centers M and M' bridged by cyanide ligands to form a cubic lattice structure. The possibility to induce a reversible change in the electronic structures has stimulated much experimental and theoretical works with potential applications in information storage devices. A variety of magnetic interactions sprouts from the presence of 3d paramagnetic ions connected by cyano bridges, ranging from room-temperature magnets[5,6] to single-molecule magnets.[7]

A prominent representative of this family of compounds is the Co(III)-Fe(II) PBA which undergoes a diamagnetic-ferrimagnetic transition to Co(II)-Fe(III) upon irradiation. However, it is difficult to describe the electronic structure and spectroscopy of these PBAs due to the presence of intermingled physical and structural phenomena. The global transition involves spin transition on the M site and electron transfer and magnetic interaction between the M and M' sites. Furthermore, the energy ordering can be modified by varying the crystal field (*i.e.*, nature of the ligands) and the environment (*i.e.*, Madelung field) generated by the presence of vacancies, water molecules and inserted alkali ions[8]. It has been suggested that electron transfer is triggered by the displacement of the Co(III) ion in the presence of a water molecule.[9]

At this stage, let us stress that certain PBA matrices are also remarkable hosts for alkali ions. Indeed, M-CN-M' units have been recently considered as potential cathodes for Na^+-ion based batteries. Compounds of chemical formula $KM[Fe(CN)_6]\cdot zH_2O$ (M = Mn, Fe, Co, Ni, Zn) have demonstrated promising capacities thanks to the large interstitial spaces that offer reversible insertion and mobility.[10–12] The possibility to replace Li^+ ions by Na^+ ions in traditional batteries is of particular importance considering the lithium demand.

The complexity in PBAs stems from intermingled structural modifications within the lattice, electron transfers reactions, and magnetic properties modifications. Thus, a systematic inspection of PBAs electronic structures seems out of reach using state-of-the-art *ab initio* methods. In that sense, the Ni(II)-Fe(III) PBA turns out to be a relevant candidate since electron transfer has not been stressed out whereas magnetic interaction between paramagnetic centres is anticipated to be the predominant phenomenon.

In this work, our goal is to investigate the speculated ferromagnetic-to-antiferromagnetic transition in the Ni(II)-Fe(III) PBA by means of wave function-based calculations. Indeed, the relationship between structural deformations (see Figure 1) and the electronic structure is of prime importance in order to understand the resulting macroscopic properties. In strong analogy with proton-coupled electron transfer (PCET) processes,[13–15] one can anticipate that the intersite electron

[a]*Laboratoire de Chimie Quantique, Université de Strasbourg, 1 Rue Blaise Pascal, 67000 Strasbourg, France, E-mail: tim.krah@etu.unistra.fr,vrobert@unistra.fr*
[b]*Laboratoire de Chimie et Physique Quantiques, 118 Route de Narbonne, 31062 Toulouse Cedex 09, France*

transfer amplitude is related to the reported Na^+-ions mobility in a unified "cation-coupled electron transfer" (CCET) picture. Such original concept is of particular importance in PBAs which combine magnetic and valence tautomerism properties.

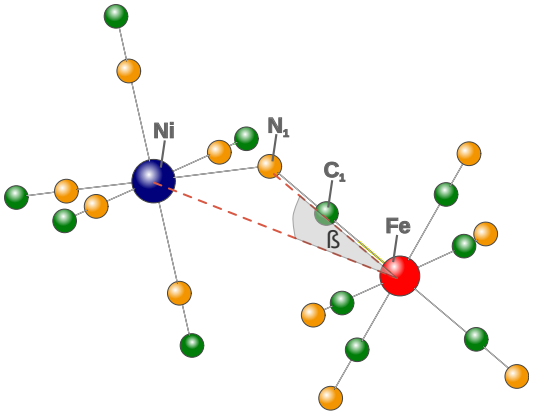

Fig. 1 Representation of the $Ni(II)(NC)_5$-N_1C_1-$Fe(III)(CN)_5$ cluster. The rotation of the $Ni(NC)_5$ and the rigid $Fe(CN)_6$ unit in opposite directions leads to the opening of the bridging C_1N_1 ligand. This structural deformation is measured by the angle β.

2 Theoretical Details

The magnetic interactions in the NiFe compound are governed by the overlap of the magnetic orbitals on the Ni and Fe centers and the σ, π and π^* orbitals of the bridging C_1-N_1 cyanide ligand. It is known from experiments that the $Fe(CN)_6$ unit is rather rigid [16,17] whereas distortions are likely to occur around the Ni center. Indeed, X-ray diffraction measurements performed under high pressure conditions have suggested the existence of a weakness in PBAs lattices around the divalent ion, namely Ni(II). Therefore, the opening of the bridging C_1N_1 ligand along the angle β (see Figure 1) is a relevant deformation which is expected to modify the orbital overlap, and as a result the exchange interactions between the paramagnetic centers.

We followed the commonly employed embedded cluster approach [9,18] in order to treat a molecular cluster using accurate wave function based calculations while still taking into account the leading effects of the actual crystalline surrounding. In this case, the molecular cluster is defined as the magnetic centers and their respective first coordination spheres, that is, the $Ni(II)(NC)_5$-N_1C_1-$Fe(III)(CN)_5$ system, called NiFe cluster hereafter. All-electron basis functions were introduced on all atoms of this NiFe cluster. Namely, we used the recently developed atomic natural orbital ANO-RCC basis sets [19,20] with the following contractions, commonly accepted for studies of magnetic systems: [9] Fe, Ni (5s4p2d); C,N (3s2p1d).

The rest of the crystal can be divided into a short-range and a long-range region. First, the short-range embedding (up to the first cluster neighbours) contains 10 total ion pseudopotentials (TIPs) on the Ni(II) and Fe(III) ions that account principally for the Pauli exclusion zones in the actual cluster proximity. Then, formal point charges [Fe(3+), Ni(2+), C(-0.5), N(-0.5)] were used to reproduce the long-range Madelung potential, a critical quantity in ionic [9,21] and molecular [22,23] crystals. Using this approach, a rectangular box of approximately 10 Å×10 Å×15 Å containing TIPs and formal point charges was considered around the central NiFe cluster (see Figure 2). It must be noticed that only a negligible computational cost is added when taking into account the embedding while the computational effort is focused on the treatment of the electronic structure of the cluster.

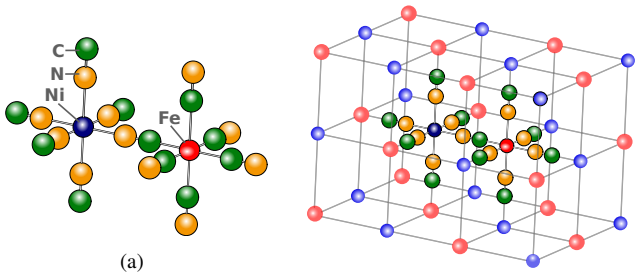

Fig. 2 (*a*) $Ni(II)(NC)_5$-N_1C_1-$Fe(III)(CN)_5$ cluster used for the DDCI calculations (*b*) embedded cluster in the NiFe PBA lattice. Embedding CN bridges are represented as grey lines for clarity.

The cluster atoms, TIPs and point charges were located at the crystallographic positions reported by Kuwabara *et al.* [24], associated with the following bond distances : d(Ni-N)=2.03 Å, d(CN)=1.15 Å and d(FeC)=1.93 Å. During the cluster deformation the TIPs and point charges remain on their crystallographic positions. The deformation was carried out by increasing the angle β (see Figure 1) from 0 to 25° in 5°-steps. All the Ni(II) and Fe(III) ions were maintained on their crystallographic positions and the rigid $Fe(CN)_6$ unit was rotated while keeping a constant angle $\angle(Fe-C_1-N_1) = 180°$. Consequently, the Ni-$N_1$ bond distance was stretched up to 2.66 Å at the maximum angle value $\beta = 25°$.

Based on this embedded cluster model, the electronic correlation can be divided into static and dynamic contributions. The former results from degenerate or quasi-degenerate electronic configurations in the presence of singly occupied molecular orbitals (MOs). In contrast, the latter captures the instantaneous electron-electron interactions. The static correlation is introduced by complete active space self-consistent field (CASSCF) [25] calculations using the 7.8 release of the

MOLCAS package.[26] As expected from the large CN^- crystal field parameter and confirmed experimentally,[27] the Fe(III,d^5) ion is in a low-spin configuration $S_{Fe} = 1/2$ and exhibits one singly-occupied 3d orbital of t_{2g}-type. The Ni(II,d^8) ion has two singly occupied 3d orbitals of e_g-type, resulting in $S_{Ni} = 1$. Consequently, a minimal active space consisting of 3 electrons in 3 orbitals (CAS[3,3]) was used (see Figure 3).

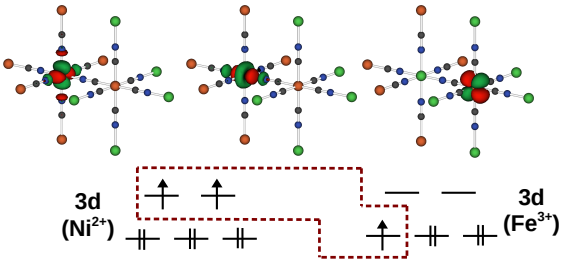

Fig. 3 The CAS[3,3] (dashed red line) used in the calculations and the corresponding Ni(II) (left) and Fe(III) (right) magnetic orbitals. The represented spin configuration corresponds to a quartet state.

Subsequently, difference dedicated configuration interaction (DDCI) calculations[28] as implemented in the CASDI code[29] incorporate the dynamic correlation through a selected CI involving orbitals of higher quantum numbers. The active space was extended to check that the remaining 3d orbitals remain with occupation numbers very close to 2.0. Besides, the DDCI wavefunction projection onto the CAS[3,3]SCF reference remains larger than 90%, supporting the validity of the active space. The DDCI method has proven to be particularly efficent in the evaluation of exchange coupling constants in molecular[30] as well as solid-state systems.[31,32] Following the DDCI approach, a single set of MOs for one particular geometry is used for all calculated states - a strategy particularly adapted to magnetic systems which usually do not exhibit large electronic reorganisation. The method introduces excited configurations (*i*) generating holes (h) and particles (p) in the inactive and virtual MOs, respectively, and (*ii*) leaving out the demanding 2h-2p class of determinants. In the following, we will refer to DDCI values for calculations performed at the DDCI-3 level (up to 2h-1p and 1h-2p classes). Let us mention that other strategies have been reported to reduce the CI space,[33], to incorporate the correlation effects which contribute to a reduction of the on-site repulsion[34] and to optimize the set of MOs used in the configurations construction.[35,36] All our calculations were carried out in the C_s point group.

3 Results and Discussion

3.1 Analytical description

The local spins can be either $S_{Ni} = 1$ or $S'_{Ni} = 0$ on the Ni center, and $S_{Fe} = 1/2$ on the Fe site. From the field generated by the cyano ligands, the local singlet state $S'_{Ni} = 0$ lies much higher in energy. Thus, we assume a local triplet and doublet state on the Ni and Fe centers, respectively. Therefore, the total spin S_{tot} of the model cluster ranges from $|S_{Ni} - S_{Fe}| = 1/2$ to $S_{Ni} + S_{Fe} = 3/2$. In the following, we derive the analytical expression for the energy difference ΔE between the doublet ($S_{tot} = 1/2$) and quartet ($S_{tot} = 3/2$) states (see Figure 3). The magnetic orbitals on the Ni and Fe centers are referred to as a,a' and b, respectively. In a first step, we only consider determinants that preserve the number of electrons on each metal center (*i.e.* "neutral determinants"), namely

$$\phi_N = |aa'\bar{b}|; \quad \phi'_N = \frac{|a\bar{a}'b| + |\bar{a}a'b|}{\sqrt{2}}.$$

In this 2×2 space, the energy difference between the doublet and quartet states ΔE_N reads

$$\Delta E_N = 2\sqrt{2}K_{ib} \tag{1}$$

where $K_{ib} = (ib,bi) = \langle i\bar{b}|\hat{H}|b\bar{i}\rangle$ ($i = a,a'$) is the exchange integral between the two magnetic sites. We assume here that $K_{ab} = K_{a'b}$.

In a second step, configurations that account for electron hopping from one site to the other (*i.e.* "ionic determinants") are included to enlarge the representation space. Such ionic forms can be written as

$$\phi_I^{Ni1} = |a\bar{a}a'|; \phi_I^{Ni2} = |aa'\bar{a}'|; \phi_I^{Fe1} = |ab\bar{b}|; \phi_I^{Fe2} = |a'b\bar{b}|.$$

The corresponding hopping integrals t_{ab} and $t_{a'b}$ connect neutral to ionic forms as

$$t_{ab} = \langle a\bar{a}a'|\hat{H}|\bar{a}a'b\rangle; \quad t_{a'b} = \langle aa'\bar{b}|\hat{H}|ab\bar{b}\rangle,$$

One should recall that the amplitude of the hopping integrals is proportional to the overlap between the magnetic orbitals. Following a perturbative treatment of the energies, the inclusion of the above ionic determinants ϕ_I leads to a relative stabilisation of the doublet state with respect to the quartet state

$$\Delta E_I = \frac{4\sqrt{2}}{3}(t_{ab}^2 + t_{a'b}^2)\left(\frac{1}{U_a} + \frac{1}{U_b}\right) \tag{2}$$

where U_a and U_b stand for the on-site electron-electron repulsion, $U_i = (ii,ii) = \langle i\bar{i}|\hat{H}|i\bar{i}\rangle$. Equations 1 and 2 can be combined to give rise to the doublet-quartet energy splitting

$$\Delta E = 2\sqrt{2}\,K_{\text{eff}} - \frac{4\sqrt{2}}{3}\,\frac{t_{\text{eff}}^2}{U_{\text{eff}}} \tag{3}$$

where $t_{\text{eff}}^2 = t_{ab}^2 + t_{a'b}^2$ and $\frac{1}{U_{\text{eff}}} = (\frac{1}{U_a} + \frac{1}{U_b})$. K_{eff} is the effective exchange integral assumed to be unique whatever a or a'. As expected, two competing contributions can be identified. The first part of equation 3 favours a ferromagnetic coupling between the two sites whereas the second part favours an antiferromagnetic behaviour. The impact of the latter depends on the ratio of the effective hopping integral t_{eff} and the effective on-site repulsion U_{eff}.

3.2 Numerical Results

The spin-Hamiltonian

$$H = -JS_{\text{Ni}} \cdot S_{\text{Fe}} \tag{4}$$

first introduced by Heisenberg[37] and later discussed by Dirac and Van Vleck[38] introduces the so-called exchange coupling constant J.[39] Such model Hamiltonian relies on this single parameter J, and describes the interaction between two spins, $S_{\text{Ni}} = 1$ and $S_{\text{Fe}} = 1/2$ localized on the Ni and Fe centers, respectively. J is uniquely determined by the doublet and quartet states energies and reads

$$J = \frac{1}{3}\left[E(S_{\text{tot}} = 1/2) - E(S_{\text{tot}} = 3/2)\right] \tag{5}$$

Besides, J can be split into ferromagnetic (FM) J_{FM} and antiferromagnetic (AFM) J_{AFM} contributions

$$J = J_{FM} + J_{AFM} \tag{6}$$

in correspondance to the first and second part of the analytical expression 3. The calculated J values as a function of the deformation angle β are summarized in Table 1 and represented in Figure 4.

Table 1 CAS-CI (CI) and CAS-DDCI (DDCI) calculated exchange coupling constants (cm^{-1}) with respect to the deformation angle β (°) (see Figure 1). The set of MOs used in the DDCI calculations is the quartet state one (see Figure 3).

Angle β (°)	J_{CI} (cm^{-1})	J_{DDCI} (cm^{-1})
0	+1.8	+11.4
5	+1.2	+7.4
10	-0.4	-1.1
15	-1.7	-10.0
20	-2.1	-12.4
25	-1.5	-8.5

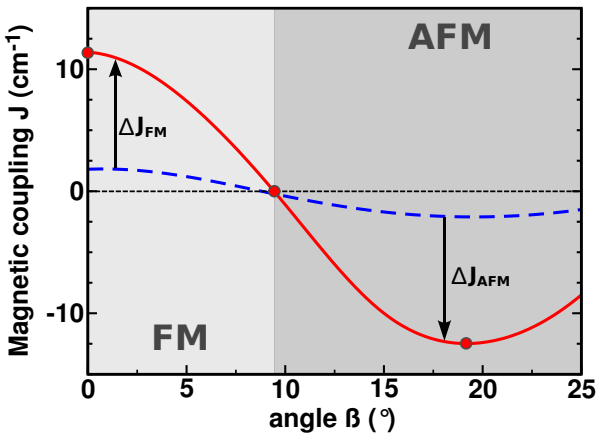

Fig. 4 Exchange coupling constant J (cm^{-1}) as a function of the deformation angle β (N_1FeNi) at CAS(3,3) (blue, dashed line) and DDCI (red, solid line) level of theory. The ferromagnetic (FM, $J > 0$) and antiferromagnetic (AFM, $J < 0$) regimes are highlighted. Red circles illustrate the positions of particular values used in the text.

Let us first discuss the J_{CI} values in Table 1. These are obtained from CAS[3,3]-CI calculations using the state-specific CAS[3,3]SCF MOs of the $S = 3/2$ state.

In the $\beta \sim 0°$ regime, the system exhibits ferromagnetic (FM) behaviour (J =+1.8 cm^{-1}). This result is a reflection of the orthogonality between the t_{2g}-like (b) and e_g-like (a, a') MOs localized on the Fe(III) and Ni(II) centers. As mentioned previously, the hopping integral t_{eff} is proportional to the overlap between these orbitals. As expected from Kahn's model, the antiferromagnetic contribution is suppressed with a vanishingly small t_{eff} value, leaving a FM behaviour (see J_{CI} values in Table 1).

As soon as the cluster is deformed, the magnetic orbital overlap is enhanced and switches on the antiferromagnetic contribution. Therefore, the J value is reduced and spans the FM regime up to a β value of 9.5° (see Figure 4). For this critical value, the Ni-N distance is 2.14 Å as compared to the reported value 2.03 Å.[24] Beyond this critical value, the system exhibits an AFM behaviour up to $\beta = 25°$, with the lowest J value of -2.1 cm^{-1} at $\beta = 20°$.

Let us now concentrate on the DDCI set of calculated values. The importance of correlation effects to reach spectroscopic accuracy has been discussed in the literature.[40,41] First, the J value of the non-deformed complex ($\beta = 0°$, J = +11.4 cm^{-1}) is consistent with the experimental Curie temperature value T_c = 24 K,[27] and therefore validates our embedded cluster DDCI calculations. It is noticeable that the same FM and AFM regimes with a common frontier at $\beta = 9.5°$ can be identified at the DDCI level. Thus, the qualitative behaviour is not modified. However, the dynamical correlation

introduced at the DDCI level greatly amplifies the height of variations, with J values ranging from +11.4 cm^{-1} at $\beta = 0°$ to -12.5 cm^{-1} at $\beta = 19°$ (see Figure 4). In the FM region, $J_{DDCI} = J_{CI} + \Delta J_{FM}$ with $\Delta J_{FM} > 0$ whereas in the AFM region $J_{DDCI} = J_{CI} + \Delta J_{AFM}$ with $\Delta J_{AFM} < 0$ (see Figure 4). In other words, the correlation effect at the DDCI level seems to stabilise whichever form of magnetic behaviour is dominant in the wave function at the CAS-CI level.

The positive character of ΔJ_{FM} deserves particular attention. Let us recall that the DDCI space includes the important 2h-1p and 1h-2p sets of excitations. For ferromagnetic systems, the wave functions are essentially represented by neutral forms. Therefore, the AF pathways involving the stabilisation of the ionic forms have a negligible contribution. At the DDCI level, the leading contribution effect is not related to the direct interaction of 2h-1p excitations with the valence-bond forms. Their ferromagnetic contribution is associated to more complex pathways involving simultaneously other types of excitations, ligand-to-metal charge transfer (LMCT) forms.[42,43]

As previously reported from selected CI calculations,[43] the presence of the 2h-1p determinants produces an enhancement of the LMCT forms. Besides, the LMCT quartet state is expected to be stabilized as compared to the doublet by Hund's rule. Therefore, the coupling between 2h-1p and the LMCT forms favours the quartet state, and consequently gives rise to a ferromagnetic contribution $\Delta J_{FM} > 0$.

This is to be contrasted with the AFM regime in Figure 4. The calculated $\Delta J_{AFM} < 0$ at the DDCI level is a reflection of the stabilisation of the ionic forms which progressively gain weight in the CAS-CI wave function. It is known from the literature that instantaneous charge reorganization (so-called dynamical correlation effects) stabilizes the ionic forms.[40] Such phenomenon is introduced beyond the CASSCF mean field picture and plays a dominant role in the spin states ordering. As a consequence, U_{eff} in Equation 3 is reduced by the introduction of dynamical correlation effects.

From the rigidity imposed to the $Fe(CN)_6$ unit, the Ni-N_1 distance is continuously stretched along the deformation. Therefore, the overlap between the Ni 3d and the bridging π orbitals is reduced, leading to an increase of J beyond the minimum value found at $\beta = 19°$. Let us mention that such regime is not realistic since the Ni-N_1 distance is stretched by more than 30%.

In order to quantify the effective hopping integral t_{eff} modulation, we finally used the DDCI J values calculated for $\beta = 0$, 9.5 and 19°, $J = 11.4$, 0 and -12.5 cm^{-1} (red circles in Figure 4). From the value at $\beta = 0°$, equation 3 leads to $K_{\text{eff}} = 4.03$ cm^{-1} since t_{eff} is negligibly small. Due the strong atomic character of the magnetic orbitals (projections on the 3d atomic orbitals are larger than 0.75 for $0° < \beta < 20°$), the K_{eff} and U_{eff} were assumed to be constant along the deformation. This assumption allows us to concentrate on the modification of the hopping integral parameter. One can easily observe that t_{eff} is increased by a factor 1.5 as the angle β is increased from 9.5 to 19°. This change in the electron transfer amplitude is expected to be coupled the cation transfer in the NiFe PBA, a mechanism of prime importance to enhance ion mobility.

4 Conclusion

Wave function-based DDCI calculations were performed on an embedded cluster to investigate the magnetic properties of the NiFe Prussian Blue Analogue. Our calculation for the non-distorted structure is consistent with the experimental Curie temperature. A rather significant change in the calculated exchange coupling constant (*i.e.*, 23.9 cm^{-1}) was observed as the local environment of the Ni center is modified away from strictly octahedral geometry. This change from ferromagnetic to antiferromagnetic behaviour can be understood as an increase of magnetic orbital overlap. In that sense, the cluster deformation switches on the effective hopping transfer t_{eff} between the magnetic centers. t_{eff} increases by a factor of $\sim$1.5 over an opening-range of $\sim 10°$ of the Ni-NC-Fe cyano bridge. In view of the proven Na^+ mobility in NiFe PBA and in analogy with PCET processes, the increase of the hopping integral should be coupled to the Na^+ ion diffusion within the matrix in a "cation-coupled electron transfer" (CCET) picture. Such a coupling could be a step towards tunable magnetic and conducting materials.

Acknowledgement

This work was supported by the International Center for Frontier Research in Chemistry (icFRC, Strasbourg) through the PhD grant of T.K.

References

1 Stahl, G. E. *Experimenta, Observationes, Animadversiones CCC Numero, Chymicae et Physicae* **1731**, 281–283

2 Dei, A.; Gatteschi, D.; Sangregorio, C.; Sorace, L. *Accounts of Chemical Research* **2004**, *37*, 827–835

3 Evangelio, E.; Ruiz-Molina, D. *European Journal of Inorganic Chemistry* **2005**, *2005*, 2945–2945

4 Evangelio, E.; Bonnet, M.-L.; Cabaas, M.; Nakano, M.; Sutter, J.-P.; Dei, A.; Robert, V.; Ruiz-Molina, D. *Chemistry A European Journal* **2010**, *16*, 6666–6677

5 Mallah, T.; Thibaut, S.; Verdaguer, M.; Veillet, P. *Science* **1993**, *262*, 1554–1557

6 Ferlay, S.; Mallah, T.; Ouahs, R.; Veillet, P.; Verdaguer, M. *Nature* **1995**, *378*, 701–703

7 Cho, K. J.; Ryu, D. W.; Kwak, H. Y.; Lee, J. W.; Lee, W. R.; Lim, K. S.; Koh, E. K.; Kwon, Y. W.; Hong, C. S. *Chem. Commun.* **2012**, *48*, 7404–7406

8 Cafun, J.-D.; Champion, G.; Arrio, M.-A.; Cartier dit Moulin, C.; Bleuzen, A. *J. Am. Chem. Soc.* **2010**, *132*, 11552–11559

9 Krah, T.; Suaud, N.; Zanchet, A.; Robert, V.; Ben Amor, N. *European Journal of Inorganic Chemistry* **2012**, 5777–5783

10 Lu, Y.; Wang, L.; Cheng, J.; Goodenough, J. B. *Chem. Commun.* **2012**, *48*, 6544–6546

11 Wessells, C. D.; Peddada, S. V.; McDowell, M. T.; Huggins, R. A.; Cui, Y. *Journal of The Electrochemical Society* **2011**, *159*, A98–A103

12 Moritomo, Y.; Takachi, M.; Kurihara, Y.; Matsuda, T. *Applied Physics Express* **2012**, *5*, 041801

13 Feig, A. L.; Lippard, S. J. *Chem. Rev.* **1994**, *94*, 759–805

14 Mayer, J. M. *Annu. Rev. Phys. Chem.* **2004**, *55*, 363–390

15 Weinberg, D. R.; Gagliardi, C.; Hull, J.; Murphy, C.; Kent, C.; Westlake, B.; Paul, A.; Ess, D.; McCafferty, D.; Meyer, T. *Chem. Rev.* **2012**, *112*, 4016–4093

16 Yokoyama, T.; Ohta, T.; Sato, O.; Hashimoto, K. *Phys. Rev. B* **1998**, *58*, 8257–8266

17 Cafun, J.-D.; Lejeune, J.; Iti, J.-P.; Baudelet, F.; Bleuzen, A. *The Journal of Physical Chemistry C* **2013**, *117*, 19645–19655

18 Lepetit, M.-B.; Suaud, N.; Gelle, A.; Robert, V. *The Journal of Chemical Physics* **2003**, *118*, 3966–3973

19 Roos, B. O.; Lindh, R.; Malmqvist, P.-A.; Veryazov, V.; Widmark, P.-O. *J. Phys. Chem. A* **2004**, *108*, 2851–2858

20 Roos, B. O.; Lindh, R.; Malmqvist, P.-A.; Veryazov, V.; Widmark, P.-O. *J. Phys. Chem. A* **2005**, *109*, 6575–6579

21 Le Guennic, B.; Borshch, S.; Robert, V. *Inorganic Chemistry* **2007**, *46*, 11106–11111

22 Kepenekian, M.; Le Guennic, B.; Robert, V. *Phys. Rev. B* **2009**, *79*, 094428

23 Kepenekian, M.; Guennic, B. L.; Robert, V. *Journal of the American Chemical Society* **2009**, *131*, 11498–11502

24 Yamada, S.; Kuwabara, K.; Koumoto, K. *Materials Science and Engineering: B* **1997**, *49*, 89 – 94

25 Roos, B. O.; Taylor, P. R.; Siegbahn, P. E. *Chemical Physics* **1980**, *48*, 157 – 173

26 Karlström, G.; Lindh, R.; Malmqvist, P.-A.; Roos, B. O.; Ryde, U.; Veryazov, V.; Widmark, P.-O.; Cossi, M.; Schimmelpfennig, B.; Neograd y, P.; Seijo, L. *Comput. Mater. Sci.* **2003**, *28*, 222–239

27 Juskzykt, S.; Johansson, C.; Hansont, M.; Ratusmas, A.; Makckill, G. *J. Phys.: Condens. Matter* **1994**, *6*, 5697–5705

28 Miralles, J.; Castell, O.; Caballol, R.; Malrieu, J.-P. *Chemical Physics* **1993**, *172*, 33 – 43

29 Ben Amor, N.; Maynau, D. *Chemical Physics Letters* **1998**, *286*, 211 – 220

30 Oms, O.; Rota, J.-B.; Norel, L.; Calzado, C. J.; Rousselire, H.; Train, C.; Robert, V. *European Journal of Inorganic Chemistry* **2010**, *2010*, 5373–5378

31 Terencio, T.; Bastardis, R.; Suaud, N.; Maynau, D.; Bonvoisin, J.; Malrieu, J. P.; Calzado, C. J.; Guihery, N. *Phys. Chem. Chem. Phys.* **2011**, *13*, 12314–12320

32 Chang, C.; Calzado, C. J.; Amor, N. B.; Marin, J. S.; Maynau, D. *The Journal of Chemical Physics* **2012**, *137*, 104102

33 Neese, F. *J. Chem. Phys.* **2003**, *119*, 9428–9443

34 Fink, K.; Staemmler, V. *Mol. Phys.* **2013**, *111*, 2594–2605

35 Angeli, C.; Calzado, C. J. *The Journal of Chemical Physics* **2012**, *137*, 034104

36 Rota, J.-B.; Le Guennic, B.; Robert, V. *Inorg. Chem.* **2010**, *49*, 1230–1237

37 Heisenberg, W. *Z. Phys* **1928**, *49*, 619

38 Dirac, P. A. M. *The Principles of Quantum Mechanics*, 3rd ed.; Clarenden, Oxford, 1947; Vol. Chap. IX

39 Verdaguer, M.; Robert, V. In *Comprehensive Inorganic Chemistry {II} (Second Edition)*, second edition ed.; Reedijk, J., Poeppelmeier, K., Eds.; Elsevier: Amsterdam, 2013; pp 131 – 189

40 Calzado, C. J.; Cabrero, J.; Malrieu, J. P.; Caballol, R. *The Journal of Chemical Physics* **2002**, *116*, 2728–2747

41 Calzado, C. J.; Cabrero, J.; Malrieu, J. P.; Caballol, R. *The Journal of Chemical Physics* **2002**, *116*, 3985–4000

42 Calzado, C. J.; Angeli, C.; Taratiel, D.; Caballol, R.; Malrieu, J.-P. *The Journal of Chemical Physics* **2009**, *131*, 044327–044340

43 Rota, J.-B.; Calzado, C. J.; Train, C.; Robert, V. *The Journal of Chemical Physics* **2010**, *132*, 154702